Substantial changes of chemical composition and sources of fine particles during the period of COVID-19 pandemic in Taiyuan, Northern China

Yang Wang[1] · Yanping Wen[2] · Yang Cui[1] · Lili Guo[1] · Qiusheng He[1] · Hongyan Li[1] · Xinming Wang[3]

Abstract

To better understand the effects of COVID-19 on air quality in Taiyuan, hourly in situ measurements of $PM_{2.5}$(particulate matter with an aerodynamic diameter less than 2.5 mm) and chemical components (water-soluble ions, organic carbon (OC), elemental carbon (EC), and trace elements) were conducted before (P1: 1 January–23 January 2020) and during (P2: 24 January–15 February 2020) the coronavirus disease 2019 (COVID-19) outbreak. The average concentrations of $PM_{2.5}$ dropped from 122.0 μg/m^3 during P1 to 83.3 μg/m^3 during P2. Compared with P1, except for fireworks burning–related chemical components (K^+, Mg^{2+}, K, Cu, Ba), the concentrations of other chemical components of $PM_{2.5}$ decreased by14.9–69.8%. Although the large decrease of some emission sources, fireworks burning still resulted in the occurrence of pollution events during P2. The analysis results of positive matrix factorization model suggested that six $PM_{2.5}$ sources changed significantly before and during the outbreak of the epidemic. The contributions of vehicle emission, industrial process, and dust to $PM_{2.5}$ decreased from 23.1%, 3.5%, and 4.0% during P1 to 7.7%, 3.4%, and 2.3% during P2, respectively, whereas the contributions of secondary inorganic aerosol, fireworks burning, and coal combustion to $PM_{2.5}$ increased from 62.0%, 1.8%, and 5.5% to 71.5%, 9.0%, and 6.2%, respectively. The source apportionment results were also affected by air mass transport. The largest reductions of vehicle emission, industrial process, and dust source were distinctly seen for the air masses from northwest.

Keywords COVID-19 · $PM_{2.5}$ · Chemical composition · Source apportionment · Regional transportation

Highlights 1.The effects of COVID-19 of $PM_{2.5}$ chemical species and sources were reported.

2.Pollution events still occurred during the Spring Festival and Lantern Festival.

3.The vehicle emissions contribution decreased by 80.9% during the COVID-19 pandemic.

4.Largest reduction of industrial process was seen for the air masses from northwest.

✉ Yang Cui
cuiyang201110@163.com

1   School of Environmental Science and Engineering, Taiyuan University of Science and Technology, Taiyuan 030024, China

2   Taiyuan Center of Ecological and Environmental Monitor, Shanxi province, Taiyuan, China

3   State Key Laboratory of Organic Geochemistry, Guangzhou Institute of Geochemistry, Chinese Academy of Sciences, Guangzhou, China

Introduction

The coronavirus disease 2019 (COVID-19) that broke out in the first half of 2020 is a global infectious disease and spread rapidly all over the world. According to the report from World Health Organization (WHO), up to 4 June 2021, the global epidemic has resulted in 171,782,908 confirmed cases of COVID-19 and 3,698,621 deaths (https://covid19.who.int/). In China, to prevent the spread of the disease, Wuhan in Hubei province first announced a lockdown on 23 January 2020, followed by other provinces in mainland China (Cui et al. 2020; Na et al. 2020). After the pandemic outbreak, a series of control measures have been taken to prevent the further spread of the epidemic across the country, such as home quarantine, factories shutdown, and traffic restrictions. These control measures had indeed improved the air quality in some cities of China (Chu et al. 2021; Faridi et al. 2020; Navinya et al. 2020; Zhang et al. 2020a; Zheng et al. 2020).

This special period also could provide an unprecedented opportunity to accurately assess how the reduction in source

emissions influences the air quality. Previous studies have revealed that the control measures during the COVID-19 period have different effects on the air quality in different provinces of China (Zhang et al. 2020b). The observation of satellite and ground-based in China indicated that up to 90% reduction of certain emission during the city lockdown period could be identified (Le et al. 2020). During the epidemic control period, the average $PM_{2.5}$ concentrations decreased by 50% in the Pearl River Delta (Wang et al. 2021), an average reduction of 47% of $PM_{2.5}$ was observed in Hangzhou (Qi et al., 2021), and the $PM_{2.5}$ concentrations of Tangshan decreased by 15% (Li et al. 2020b). The contribution of industrial sources and coal combustion to $PM_{2.5}$ in Tangshan decreased from 28.9 and 11.8% before the epidemic control period to 21% and 10% during the epidemic control period, respectively. The reduction of emission sources during the epidemic period led to the decrease of pollutants levels, especially for vehicle emission and industrial process (Fan et al. 2020; Zhang et al. 2020b). Therefore, the key of reducing $PM_{2.5}$ concentrations and improving air quality is to control these main pollution sources.

However, most of the previous studies were conducted in Beijing-Tianjin-Hebei region, Yangtze River Delta, and Pearl River Delta. There are a few related studies in Shanxi. As the capital city of Shanxi, the air quality in Taiyuan in 2020 ranked the third from the bottom among 168 key cities in China, according to the comprehensive evaluation index of ambient air quality (http://www.mee.gov.cn/). Many energy-intensive industries are located in Taiyuan, including coal-fired power plants, steel smelters, and coking plants (Li et al. 2020a; Zhang et al. 2020c). The number of civil automobiles in Taiyuan reached 1.8 million by the end of 2020 (http://www.stats.gov.cn/). Although Wang et al. (2020) conducted a comparative study on many cities

in China including Taiyuan during the COVID-19 epidemic period, the sources of pollutants and the causes of heavy pollution processes were not discussed. To better understand the effects of COVID-19 on air quality in Taiyuan, hourly concentration of $PM_{2.5}$-related components (water-soluble ions, OC, EC, and trace elements) was measured before and during the COVID-19 outbreak at an urban site in Taiyuan. Hourly time-resolution measurement was adequate to reflect the process of pollution formation in detail. Positive matrix factorization model (PMF), concentration-weighted trajectory (CWT), and backward trajectory were used to explore the detailed effects of lockdown in Taiyuan. The results of this study could help the government to guide the further air quality management for Taiyuan.

Materials and methods

Sampling site

Taiyuan is located in the north-central part of Shanxi Province, which lies in the western part of the heavily polluted North China Plain (Fig. 1a). The specific terrain description has been introduced in our previous study (Li et al. 2016). The related measurements were conducted during the period from 1 January 2020 to 15 February 2020 at an air quality monitoring site (37.87° N, 112.54° E) (Fig. 1b) on the roof of the laboratory building of the Environmental Science Research Institute of Taiyuan, China. The sampling site is surrounded by traffic roads, residential buildings, and commercial offices, which can represent the urban environment. There were no obvious emission sources around the sampling site.
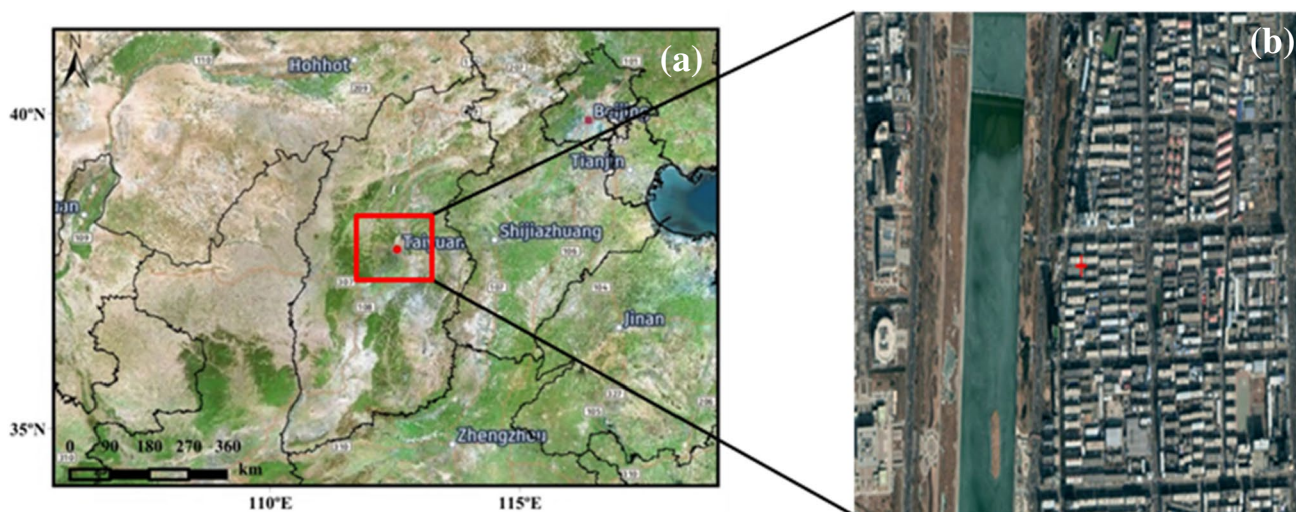

Fig.1 The topographic map of the sampling site in Taiyuan (the red dot) (**a**) and location of the sampling site (cross symbols) (**b**)

Instrument

In this study, the levels of OC and EC in $PM_{2.5}$ were measured by the RT-4 laboratory OC/EC analyzer produced by Sunset Lab in the USA. The carbon components collected on the quartz film were analyzed by thermal/optical method with a time resolution of 1 h. The concentrations of water-soluble ions in $PM_{2.5}$ including sulfate (SO_4^{2-}), nitrate (NO_3^-), ammonium (NH_4^+), sodium ion (Na^+), chloridoid (Cl^-), magnesium ion (Mg^{2+}), potassium(K^+), and calcium ion (Ca^{2+}) were monitored continuously by a model ADI 2080 online analyzer (MARGA, Metrohm Applikon) at the time resolution of 1 h. Hourly concentrations of trace elements including K, Ca, Cr, Mn, Fe, Cu, Zn, As, Se, Ba, Ni, and Pb were measured by an online multi-element analyzer (Model Xact 625, PALL Corporation, USA). The metal composition in airborne particles was measured by the standard method (X-ray photo fluorescence analysis, XF) prescribed by US EPA. The operation, calibration, and maintenance of the instrument were strictly operated according to their instruction manual. The inlet of all instruments is about 13 m above the ground. Detailed introduction on quality assurance and control (QA/QC) of instrumentation could be found in the Supporting information. Additionally, the meteorological parameters including wind direction (WD), wind speed (WS), temperature (T), relative humidity (RH), PM_{10}, $PM_{2.5}$, and trace gases (SO_2, NO_2, O_3, and CO) were acquired from the Taiyuan Environment Monitoring Central Station. PM_{10}, $PM_{2.5}$, and trace gases (SO_2, NO_2, O_3, and CO) were measured using Thermo instruments (Thermo Fisher Scientific, Franklin, Massachusetts, USA), and specific instrument models can be found in Table S3.

To ensure the validity of the data, chemical mass closure has been done which can be expressed as follows: [PM_{chem}] = [Organic matter] + [EC] + [Mineral dust] + [Trace metals] + [Sulfate] + [Nitrate] + [Ammonium] + [Chloride] (Huang et al. 2017). In this study, [OM] = 1.6 × [OC] (Cao et al. 2007; Turpin and Lim 2001). Mineral species was calculated as Mineral dust = [CaO] + [MnO_2] + [Fe_2O_3] + [K_2O] = 1.40 × [Ca] + 1.58 × [Mn] + 1.43 × [Fe] + 1.21 × [K], [Trace metals] = Ni + Cu + Pb + Zn + As + Se. Comparison of the reconstructed results and the measured $PM_{2.5}$ is shown in the Supplement (Fig. S1), and the correlation (R^2) between the measured and reconstructed $PM_{2.5}$ mass was 0.91, indicating that the data is reliable.

PMF model

The PMF model is commonly used to identify the sources of $PM_{2.5}$ and estimate the associated contributions, the USEPA PMF 5.0 model was used in this study (Huang et al. 2014; Reff et al. 2007). Detailed principle and methodology can be found in the EPA 5.0 Fundamentals and User Guide and previous study (Kim et al. 2003). The concentrations of $PM_{2.5}$, NO_3^-, SO_4^{2-}, NH_4^+, several trace elements (K, Ca, Cr, Mn, Fe, Cu, Zn, As, Se, Ba, Pb, Ni), OC, and EC were used for source apportionment of $PM_{2.5}$. It is worth noting that Cl^- and other elements have not been taken into account for PMF analysis since most of their atmospheric concentrations were below their method quantification limits (MDLs). In addition, to avoid redundant species, Ca^{2+} and K^+ were excluded from the dataset but Ca and K were taken into account. In this work, if the concentration is less than or equal to the method detection limit (MDL), the uncertainty (Unc) was calculated using a fixed fraction of the MDL: Unc = 5/6 × MDL; others were calculated based on the following equation:

$$Unc = \sqrt{(\text{Error Fraction} \times \text{concentration})^2 + (0.5 \times MDL)^2}$$

In this study, the error fractions of $PM_{2.5}$, OC, EC, SO_4^{2-}, NO_3^-, and NH_4^+ were estimated to be 15%, those of other species were 10%. $PM_{2.5}$ was set as the total variable. The predicted species showed good correlations with the measured species (Table S2). To estimate the uncertainty of the PMF solution, the displacement (DISP) and bootstrap (BS) method were used.

Concentration-weighted trajectory (CWT)

The potential source contribution function (PSCF) (Ashbaugh et al. 1985; Su et al. 2020) was commonly used to access the potential sources of pollutants, but this method can only reflect the proportion of pollution trajectories in each grid and cannot distinguish the differences between moderate and severe sources when $PM_{2.5}$ concentrations are slightly or much higher than the standard. In order to emphasize the spatial variation of the concentration of pollution source, the concentration-weighted trajectory (CWT) was used to calculate the potential source concentration weight of airflow trajectory in area, to show the variation of sources of $PM_{2.5}$ before and after the outbreak of the epidemic more visually. The geographic region was divided into an array of 0.5 ° × 0.5 ° grid cells. The calculation formula is as follows:

$$C_{ij} = \frac{1}{\sum_{l=I}^{M} \tau_{ijl}} \sum_{l=I}^{M} C_l \tau_{ijl}$$

where C_{ij} is the average weight concentration on the grid ij; l is the trajectory; C_{ij} is the corresponding $PM_{2.5}$ mass concentration when the trajectory l passes through the grid ij; and τ_{ijl} is the time that trajectory l stays in grid ij. The C_{ij} high-value grid area is the main external source area that contributes to the particulate pollution in Taiyuan.

Air mass backward trajectory analysis

The air-mass backward trajectories were calculated and clustered to track the transport pathways of airflow arriving in Taiyuan (37.87° N, 112.54° E) using the GIS-based software named TrajSat (Wang et al. 2009). Taking into account the life cycle of the secondary pollutants, the post-regression simulation time is set to 72 h to better reflect the true status of the airflow trajectory on the regional scale of the atmospheric boundary layer (Roig Rodelas et al. 2019; Wu et al. 2009). The backward trajectories started every hour (0:00–23:00) each day and were calculated at 500 m above ground level (AGL) using meteorological data (Global Data Assimilation System, (ftp://arlftp.arlhq.noaa.gov/pub/archives/gdas1/)) during the study period.

Results and discussion

Variations of concentrations of gaseous pollutants and $PM_{2.5}$ chemical composition

To better illustrate the significant effects of the epidemic outbreak on air quality, we divided the whole period into two periods (P1 and P2): before the epidemic outbreak (P1:1–23 January2020) and during the epidemic outbreak (P2:24 January–15 February2020). The average concentrations of $PM_{2.5}$, gaseous pollutants (SO_2, NO_2, CO, and O_3), water-soluble inorganic ions, OC, EC, and trace elements before (P1) and during (P2) the outbreak of COVID-19 were summarized in Table 1. The average concentrations of $PM_{2.5}$ changed from 122.0 μg/m³ during P1 to 83.3 μg/m³ during P2, decreased by 31.7%. The concentration of SO_2, NO_2 and CO decreased from 35.2 μg/m³, 65.3 μg/m³, and 1.7 mg/m³ to 26.9 μg/m³, 32.5 μg/m³, and 1.1 mg/m³, which decreased by 23.6%, 50.2%, and 35.3%, respectively. The largest

decrease in NO_2 was related to the large decrease in traffic volume during P2, which will be discussed in the "Source apportionment" and "CWT analysis of $PM_{2.5}$ sources" sections. However, the concentration of O_3 increased from 22.4 to 54.1 μg/m³, increased by 141.5%. SO_4^{2-}, NO_3^-, and NH_4^+ were the three dominant ions in $PM_{2.5}$, the total concentrations accounted for 44.8% and 45.7% of $PM_{2.5}$ during P1 and P2, respectively. The average concentrations of SO_4^{2-}, NO_3^-, and NH_4^+ decreased from 22.0 μg/m³, 17.7 μg/m³, and 15.0 μg/m³ during P1 to 14.0 μg/m³, 13.7 μg/m³, and 10.4 μg/m³ during P2, decreased by 36.4%, 22.6%, and 30.7%, respectively. The concentrations of the other three ions Cl^- (69.2%), Na^+(50.0%), and Ca^{2+}(42.9%) suffered from dramatic decreases, while the concentration of K^+(80.0%) and Mg^{2+}(185.7%) increased during P2. The concentrations of some elements K, Cu, and Ba also increased by 80.9%, 34.0%, and 148.3%. Previous studies have reported that K, Cu, Mg, and Ba were fireworks burning–related elements (Kong et al. 2015), indicating that the Taiyuan was still affected by fireworks burning during the Spring Festival and Lantern Festival. As for the other elements, the concentrations of Ca, Cr, Mn, Fe, Zn, As, Se, Ni, and Pb during P2 decreased by approximately 57.3%, 46.5%, 49.6%, 46.0%, 43.7%, 47.8%, 18.4%, 37.8%, and 38.8%, respectively; shutdown of industry and construction sites was an important reason for the reduction of these elements. OC in $PM_{2.5}$ can be derived from both primary emissions and secondary formation (Huang et al. 2014), while EC is mainly from primary emission (Bond et al. 2013; Cao et al. 2013). OC and EC during P2 decreased by 15.2% and 65.7%, respectively. The wind rose diagram in P1 and P2 (Fig. S4) showed that the WS and WD of P1 and P2 have no obvious change, and the average WS during P1 and P2 is 1.5 m/s and 1.7 m/s, respectively. Therefore, it showed that the reduction of these pollutants during P2 was mainly due to the reduction of pollution source emissions.

Table 1 Mean and standard deviation (SD) of the five criteria air pollutants (μg/m³), CO(mg/m³) and main $PM_{2.5}$ chemical species including water-soluble ions (μg/m³), trace elements (ng/m³), OC and EC (μg/m³) during P1 and P2

Variables	P1 Mean ± SD	P2 Mean ± SD	Variables	P1 Mean ± SD	P2 Mean ± SD
$PM_{2.5}$	122.1 ± 67.2	83.3 ± 54.6	K	929.3 ± 430.4	1681.5 ± 2573.0
Na^+	0.6 ± 0.4	0.3 ± 0.2	Ca	490.4 ± 442.5	209.6 ± 114.3
K^+	0.5 ± 0.4	0.9 ± 1.8	Cr	43.9 ± 49.3	23.5 ± 37.7
Mg^{2+}	0.07 ± 0.2	0.2 ± 0.3	Mn	76.2 ± 60.7	38.4 ± 39.3
Ca^{2+}	0.7 ± 0.8	0.4 ± 0.4	Fe	974.4 ± 692.0	525.9 ± 469.1
Cl^-	2.6 ± 2.0	0.8 ± 1.8	Cu	20.3 ± 23.1	27.2 ± 49.0
NH_4^+	15.0 ± 11.8	10.4 ± 7.4	Zn	181.4 ± 110.5	102.2 ± 68.2
NO_3^-	17.7 ± 10.4	13.7 ± 9.1	As	17.8 ± 15.9	9.3 ± 6.2
SO_4^{2-}	22.0 ± 23.7	14.0 ± 11.6	Se	10.3 ± 6.0	8.4 ± 5.0
Ba	38.3 ± 36.4	95.1 ± 193.2	Ni	11.9 ± 19.1	7.4 ± 15.0
Pb	102.4 ± 67.3	62.7 ± 44.6	OC	16.5 ± 7.3	14.0 ± 8.8
EC	3.5 ± 2.6	1.2 ± 1.1	SO_2	35.2 ± 20.0	26.9 ± 17.5
NO_2	65.3 ± 22.5	32.5 ± 13.6	CO	1.7 ± 0.6	1.1 ± 0.4
PM_{10}	162.0 ± 77.7	106.5 ± 59.1	O_3	22.4 ± 20.1	54.1 ± 27.7

Pollution events analysis during P1 and P2

The outbreak of the epidemic led to a sharp drop in the concentrations of pollutants in many places in China (Fan et al. 2020). In this study, when the hourly concentration of $PM_{2.5}$ more than 24 consecutive hours exceeds 150.0 μg/m³, the period was defined as a pollution event. Finally, three pollution events E1 (1.9–1.13), E2 (1.24–1.26), and E3 (2.6–2.9) were selected (Fig. 2). During E1, the maximum daily average concentration of $PM_{2.5}$ was 250.4 μg/m³ on 12 January, and the hourly concentration could reach 358 μg/m³ at 19:00 on 12 January. This pollution event can be further divided into two pollution processes. From 12:00 on 9 January to 11:00 on 10 January, the hourly concentration of $PM_{2.5}$ was higher than 150 μg/m³. From 12:00 on 10 January, with the increase of WS, the pollutant concentration decreased rapidly in a short time. From 15:00 on 11 January to 7:00 on 13 January, the hourly concentration of $PM_{2.5}$ exceeded 150 μg/m³ for 41 consecutive hours. At 15:00 on 13 January, the WS from the northeast wind rose to 2.0 m/s, and the concentration of $PM_{2.5}$ dropped to less than

100 μg/m³. During E1, SO_4^{2-}, NO_3^-, and NH_4^+ were the main ions in $PM_{2.5}$, the average concentrations were 46.9 μg/m³, 22.8 μg/m³, and 25.5 μg/m³, respectively, and the sum of the average concentrations accounted for 52.5% of $PM_{2.5}$. When the hourly concentration of $PM_{2.5}$ reached 358.0 μg/m³, the proportion of SO_4^{2-}, NO_3^-, and NH_4^+ in $PM_{2.5}$ was 59.3%. Many previous studies have shown that the conversion of precursor gases is the main source of these three ions under low T and high RH in winter (Zheng et al. 2015). The molar ration of sulfate or nitrate to sum of sulfate and SO_2 or nitrate and NO_2 could be used as the indicators of secondary transformation (Sun et al. 2006). During E1, SOR and NOR were 0.5 and 0.2, respectively. As for elements, K, Ca, Fe, and Zn were the four dominant elements, with average concentrations of 819.8 ng/m³, 156.0 ng/m³, 696.3 ng/m³, and 171.0 ng/m³, respectively. The average concentrations of OC and EC were 16.3 μg/m³ and 3.7 μg/m³, respectively. OC/EC can be used to evaluate the source of pollutants. When the value of OC/EC is between 1.0 and 4.2, it indicated that the carbonaceous aerosol came from vehicle exhaust emissions (Schauer et al. 2002). When the value of OC/EC is between
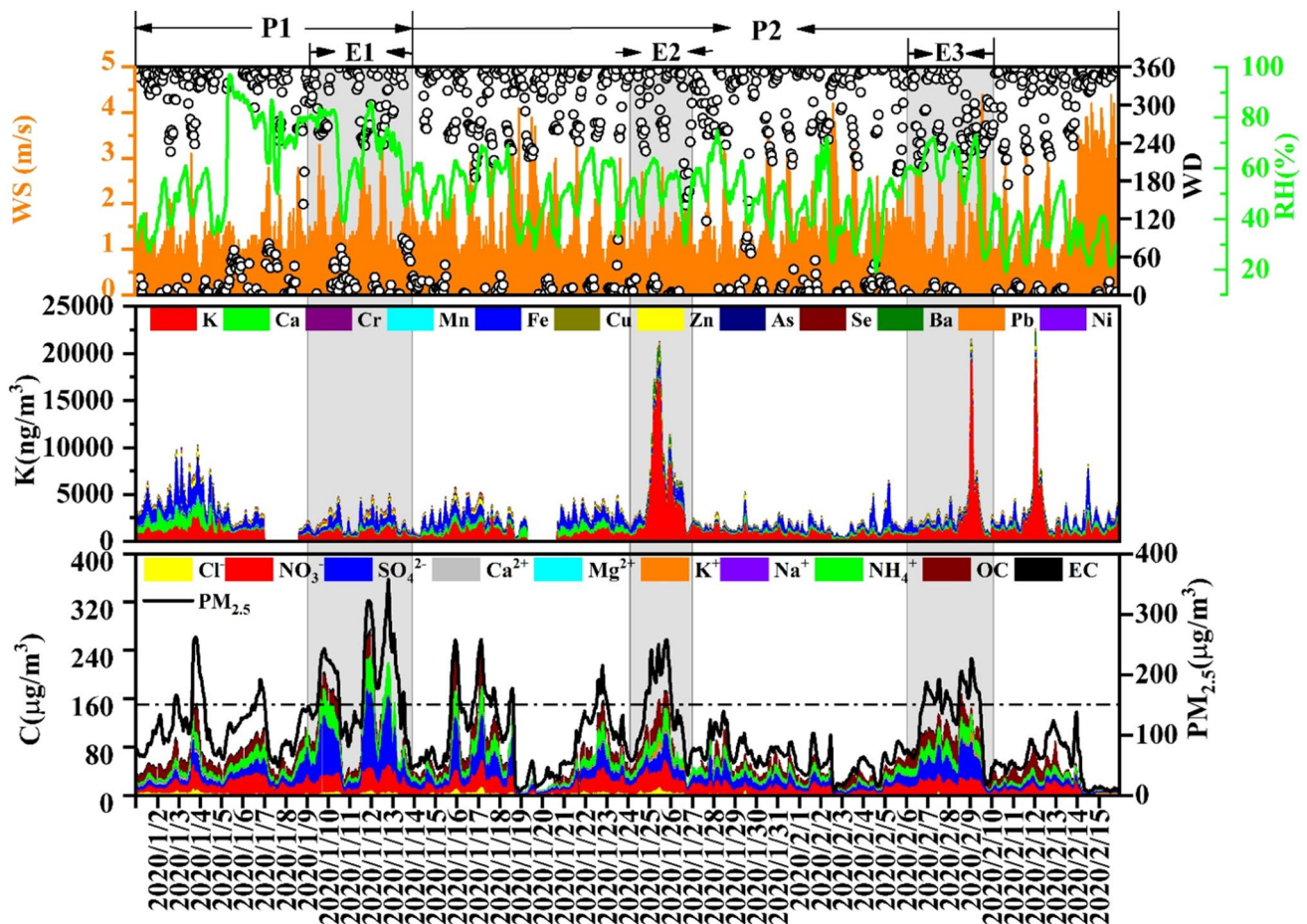

Fig.2 Time series of $PM_{2.5}$ and its major components (twelve elements, eight water-soluble ions, OC, and EC) and meteorological data (wind speed (WS), wind direction (WD), temperature (T), and relative humidity (RH)) during the study period

2.5 and 10.5, it indicates that the emission comes from coal burning. During E1, the value of OC/EC was 4.4. It can be seen that the heterogeneous reaction of gaseous pollutants, vehicle emissions, coal combustion, and road dust may be the important sources of PM$_{2.5}$ during E1.

Both E2 and E3 pollution events all occurred during P2. The average concentrations of PM$_{2.5}$ during E2 and E3 were 138.8 μg/m^3 and 135.8 μg/m^3, respectively. The hourly maximum concentrations could reach 258.0 μg/m^3 and 227.0 μg/m^3, respectively. During E2 and E3, SO$_4^{2-}$, NO$_3^-$, and NH$_4^+$ were still the main ions in PM$_{2.5}$, and the sum of these three ions accounted for 43.0% and 50.9% of PM$_{2.5}$, respectively. During E2, the concentrations of SO$_4^{2-}$, NO$_3^-$, and NH$_4^+$ were 18.5 μg/m^3, 25.3 μg/m^3, and 15.9 μg/m^3, respectively. During E3, the concentrations of SO$_4^{2-}$, NO$_3^-$, and NH$_4^+$ were 29.7 μg/m^3, 20.2 ug/m^3, and 19.2 ug/m^3, respectively; the SOR and NOR during E2 were 0.3 and 0.4, and the SOR and NOR during E3 was 0.4 and 0.3, respectively. During E2, the concentrations of K, Cu, and Ba were 4465.8 ng/m^3, 83.0 ng/m^3, and 342.3 ng/m^3, respectively, which were 5.4, 4.4, and 17.3 times higher than those during E1. K, Cu, and Ba are the reliable indicators of fireworks burning (Kong et al. 2015). Since 19:00 on 24 January, the concentrations of these three elements increased rapidly, and the hourly maximum concentrations could reach 17,201.0 ng/m^3, 279.0 ng/m^3, and 1439.0 ng/m^3 at 9:00 on 25 January. E3 occurred during the Lantern Festival. Compared with

E2, E3 is also affected by the fireworks burning. The average concentrations of elements K, Cu, and Ba were 1923.1 ng/m^3, 28.6 ng/m^3, and 73.0 ng/m^3, respectively. In addition to the impact of fireworks burning, unfavorable weather conditions (low WS and higher RH) were also the main reasons for the higher concentrations of pollutant during the pollution events (Fig. S5).

Source apportionment

In this study, PMF 5.0 was employed to conduct source apportionment. After multiple runs of different factors, six main sources of PM$_{2.5}$ were finally identified, including coal combustion, secondary inorganic aerosol, fireworks burning, dust source, industrial process, and vehicle emission. The source profiles and diurnal variations of different sources derived from the PMF model are shown in Fig. 3 and Fig. 4, respectively. BS and DISP were conducted to analyze the uncertainty of the PMF model at six factors. The results were presented in Table S1 and Table S2. As for the selected PMF solution, no swaps occurred in DISP runs (Table S1) and more than 94% of the BS runs were mapped for all factors (Table S2). Thus, the results of PMF runs were stable.

Factor 1 can be identified as the source of coal combustion (CC). Higher loadings of As and Se and moderate loading of OC and EC were found in this factor, indicting a typical source profile of CC (Liu et al. 2019;

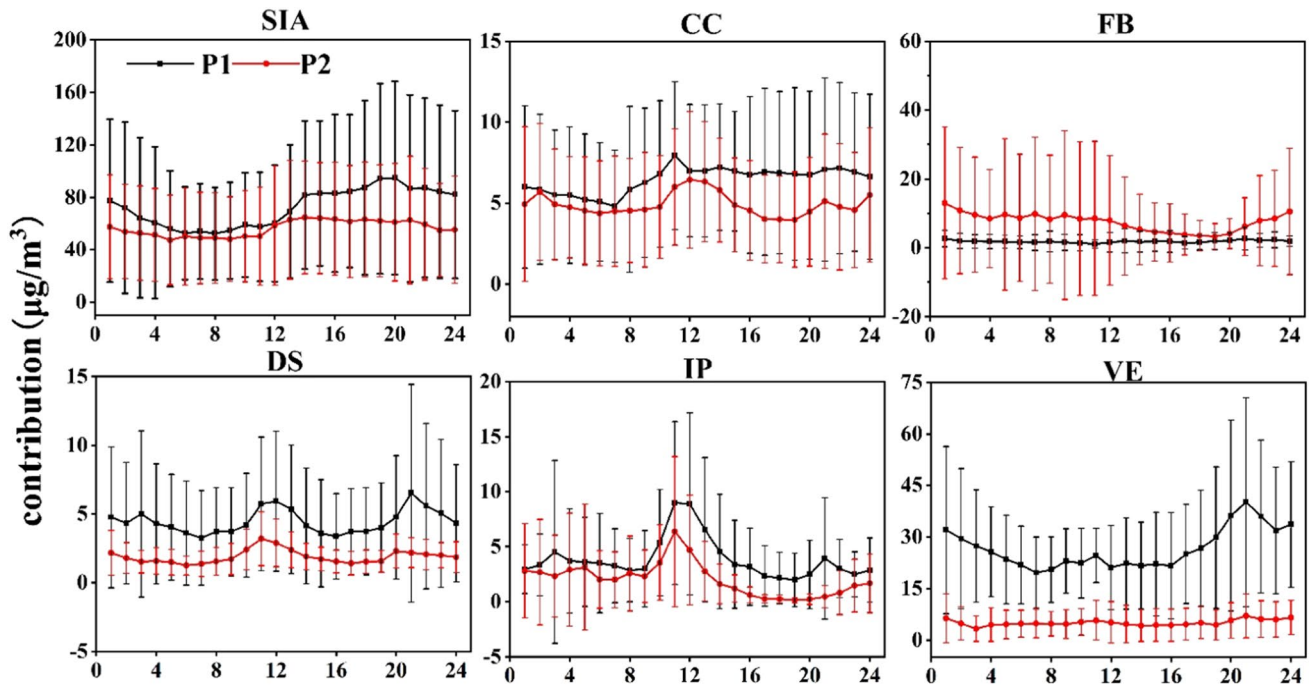**Fig.3** Factor profiles (% of species) of each source during the study period at Taiyuan
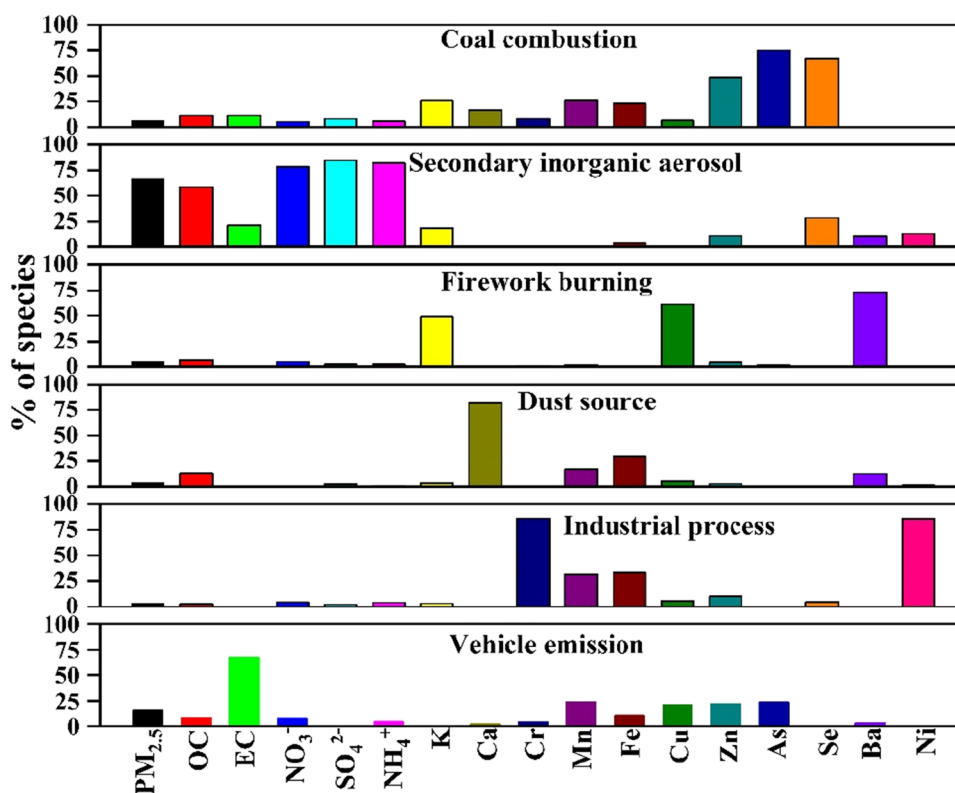
Fig.4 Diurnal variations of PM$_{2.5}$ sources derived from the PMF model during P1 and P2

Tian et al. 2015); a series of coal-electricity bases were built in Shanxi (Liu et al. 2018). Thus, it was reasonable to attribute this factor to CC. Factor 2 was characterized by higher contributions of NO$_3^-$, SO$_4^{2-}$, NH$_4^+$, and OC (Lyu et al. 2016; Zheng et al. 2019), and this factor can be identified as secondary inorganic aerosol (SIA). Factor 3 can be identified as the source of fireworks burning (FB). K, Cu, and Ba accounted for the largest proportion in this factor. According to some previous studies, K, Cu, and Ba are used to display different colors during the process of fireworks burning (Kong et al. 2015; Rai et al. 2020). Additionally, as seen from the diurnal variation of firework burning during P2 (Fig. 7), the higher emissions of fireworks burning at night also could confirm it. The concentrations of fireworks-related elements (K, Ba, and Cu) increased rapidly during the night of New Year's Eve. Factor 4 can be identified as a source of dust source (DS). This factor was distinguished by higher loadings of crustal elements such as Ca, Fe, and Ba (Lyu et al. 2016; Su et al. 2020). In factor 5, Cr, Mn, Fe, and Ni accounted for a relatively higher proportion (Taiwo et al. 2014). As for the steel plants, a large amount of Fe and Mn were released during the production process (An et al. 2015). A large steel smelter in Taiyuan produced 10.7 million tons of steel in 2020, so this factor can be attributed to industrial processes (IP). Factor 6 can be identified as the source of vehicles emission (VE), OC, EC, Cu, and Zn accounted for the relatively higher proportions (Xia and Gao 2011; Yao et al. 2016). The diurnal variations of vehicles emissions

showed the peaks in the morning and evening during P1. The diurnal variations during P2 were not obvious due to the strict traffic control measures (Fig. 4).

After COVID-19 outbreak, the contributions of these sources varied greatly due to the implementation of strict lockdown control measures. As shown in Fig. 5, compared with P1, except for the increase for the concentration of FB, the concentrations of the other five sources during P2 all decreased. Among them, the concentrations of VE, DS, IP, SIA, and CC decreased by 80.9%, 57.4%, 47.6%, 22.3%, and 23.8%, respectively. A series of strict control measures during P2 was the direct reason for the decrease. The concentration of FB increased by the factors of three. The contribution of each source to PM$_{2.5}$ is different from the change of the concentration. The contribution of SIA showed the marked increase from 62.0 to 71.5%, and it is consistent with the previous studies during COVID-19 (Li et al. 2020b; Zheng et al. 2020). The contribution of CC also increased from 5.5 to 6.2%; the COVID-19 pandemic led to the shutdown of many industries and decreased of the CC emissions from these sectors. However, the government-enforced home order might increase the electricity consumption and coal heating, which offset the decreases of CC contributions to industrial activities to some extents (Li et al. 2020b). The contribution of fireworks burning to PM$_{2.5}$ increased from 1.8% during P1 to 9.0% during P2 because of the Spring Festival and the Lantern Festival. In order to reduce the air pollution caused by the fireworks burning during the Spring Festival, the policy of prohibiting firework burning should
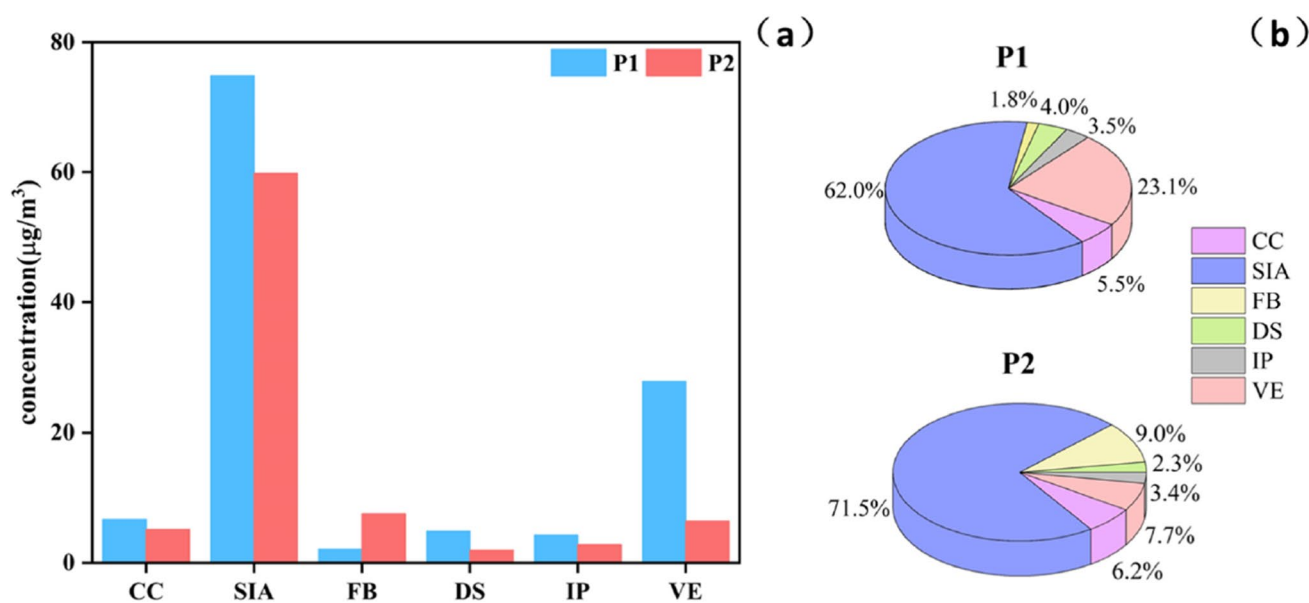
Fig. 5 The average concentrations of the identified sources (**a**) and source contributions to total PM$_{2.5}$ (b) during P1 and P2

be strictly regulated in urban areas. Strengthening the emission control of FB in rural areas should be the next priority to prevent the occurrence of heavy polluting processes during the holidays. For other three sources, contribution of VE to PM$_{2.5}$ presented the largest decrease from 23.1% during P1 to 7.7% during P2. The proportion of DS decreased from 4.0 to 2.3%. The proportion of IP decreased from 3.5 to 3.4%.

CWT analysis of PM$_{2.5}$ sources

In addition to local emissions, regional transport also could affect the concentrations of pollutants. As shown in Fig. 6, the potential source areas and relative contribution of source areas for different sources were identified by CWT. In order to reflect the effects of the epidemic more intuitively, the concentration range of the same pollution source was set to the same level. During P1, the concentrations of PM$_{2.5}$ from VE showed the higher values (> 24 μg/m^3) on the large scale. High-value areas exceeding 40 μg/m^3 were mainly distributed near the sampling point. Compared with P1, the contribution area of VE during P2 decreased significantly, and most of the spatial concentrations of PM$_{2.5}$ from VE were lower than 8 μg/m^3. Since January 24, the intensity of intra-city travel in Taiyuan decreased significantly (https://qianxi.baidu.com/2020/). Potential source areas with higher values (8–10 μg/m^3) of DS were mainly distributed in local areas during P1. With the shutdown of construction activities and the reduction of road traffic, the average concentrations from DS were lower than 2 μg/m^3 during P2 on large scale. As seen from Fig. 6, source areas of FB with lower

values (< 12 μg/m^3) during P1 only distributed in the northeastern area of Taiyuan on small scale. The higher values (> 21 μg/m^3) of FB during P2 were mainly distributed in Inner Mongolia, Shaanxi, and southwest of Shanxi. The hourly concentration could reach to 120.5 μg/m^3 at 9:00 on 25 January, and the average concentration of FB increased by 254%. As for IP, the source areas of high concentrations (6–9 μg/m^3) during P1 were mainly distributed in the southwest of the sampling point. During P2, the potential source areas of IP also reduced, and the average concentration of IP decreased by 33%, but there are still small areas of higher concentration (7–9 μg/m^3) in the northeast areas of the sampling site. The potential source region with concentrations exceeding 100 μg/m^3 of SIA during P1 mainly distributed in the northwest of sampling site, including Inner Mongolia, Shaanxi, and Shanxi Provinces. The higher value region (70–100 μg/m^3) of SIA during P2 was mainly distributed in the northwest and south of the sampling site. The average concentration decreased from 74.8 μg/m^3 during P1 to 59.8 μg/m^3 during P2, decreased by 20%. The potential source areas of CC were located in the western region of Shanxi and eastern region of Shaanxi during P1. Due to the shutdown of some industries, the CC used in industry decreased during P2, but heating and power supply were not interrupted, so the average concentration of CC only decreased by 23% during P2. The higher concentration areas of CC were mainly located in the southwest of the sampling point during P2.

During the whole study period, the air masses were classified into three clusters (Fig. 7). Source contributions of six factors for each trajectory cluster are also shown in Table 2.
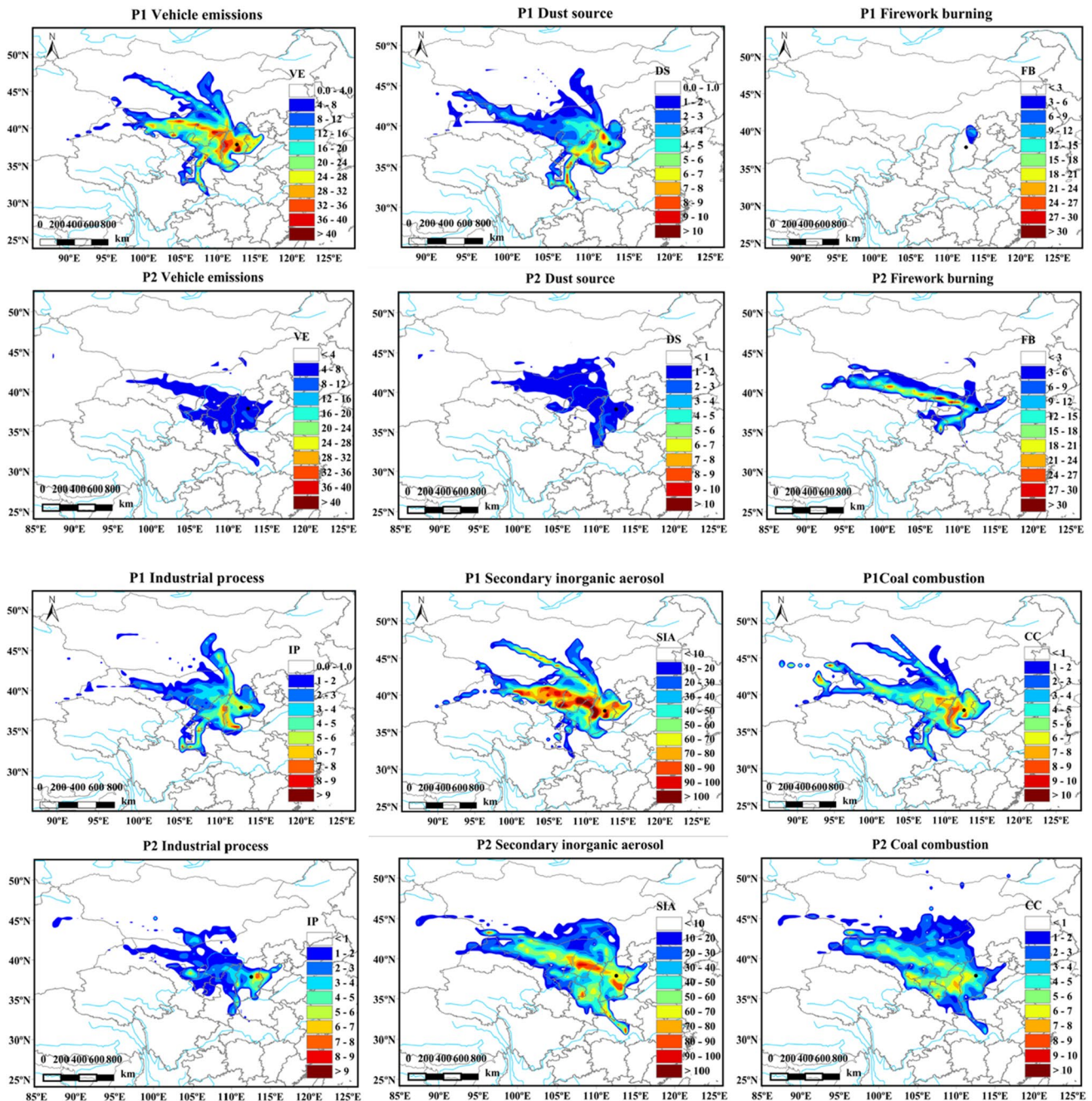
Fig.6 Concentration-weighted trajectory (CWT, µg/m³) values of source contributions during P1and P2

The air masses for Cluster 1 (C1) originated from the southern area of Shaanxi Province and passed the southwestern areas of Taiyuan; this cluster made up for 47.2% of the air masses. The air masses for Cluster 2 (C2) and 3 (C3) all came from northwest areas of the sampling site; C2 was originated from Kazakhstan near Xinjiang Uygur Autonomous Region, and C3 was originated from Mongolia; these clusters accounted for 14.3% and 38.1% of the air masses, respectively. We further analyzed the contributions of six

sources during the two periods (P1, P2) for different air mass clusters. Compared to P1, the concentrations of PM$_{2.5}$ in C1, C2, and C3 during P2 decreased by 8.9%, 35.9%, and 29.4%, respectively. As for the strict travel control measures, the contributions of VE in C1, C2, and C3 during P2 decreased by 65.3%, 79.3%, and 76.1%. Due to the shutdown of construction activities during P2, the contribution of DS decreased by 48.8%, 31.3%, and 74.2% for C1, C2, and C3, respectively. The concentration of IP decreased by

Fig.7 Cluster analysis of 72-h air-mass back-trajectories arriving at Taiyuan and concentrations of each source from different air mass clusters for the study period including P1 and P2
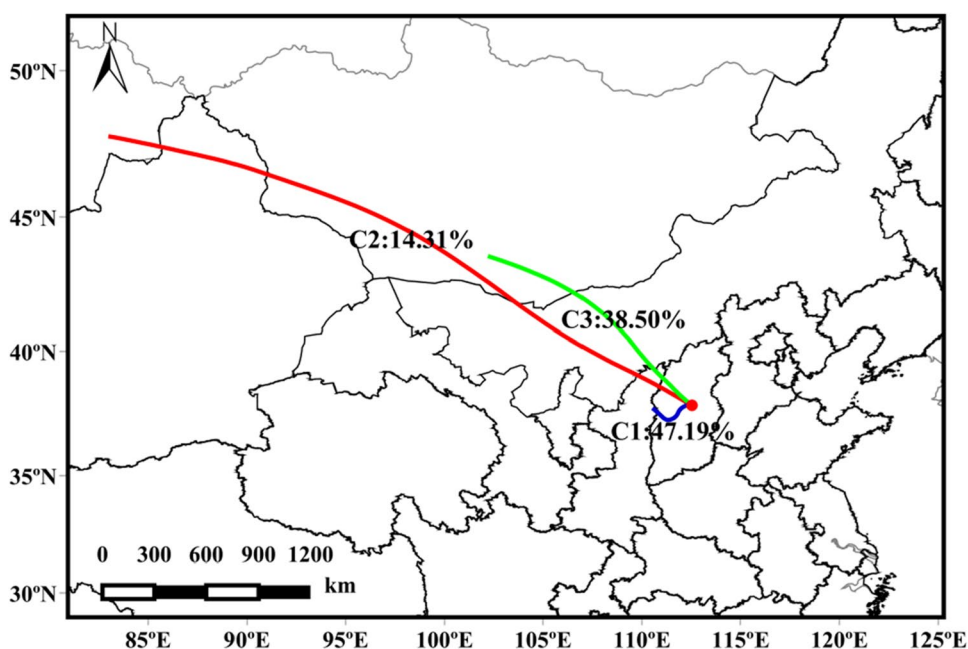
6.7%, 31.4%, and 27.8% for C1, C2, and C3, respectively. The concentrations of SIA decreased by 4.7%, 34.9%, and 8.3% for C1, C2, and C3, respectively. The concentrations of CC decreased by 42.4%, 10.6%, and 27.8% for C1, C2, and C3, respectively. In contrast to other sources, the concentrations of FB increased by 21.4%, 775.0%, and 156.0% for C1, C2, and C3, respectively. During the transport process, the carried gaseous precursors (SO_2, NO_2, NH_3) could be transformed into secondary aerosol and resulted in rapid increases of $PM_{2.5}$ concentrations in the downwind area (Bressi et al. 2014; Li et al. 2015). The concentrations of SIA on C2 and C3 were nearly twice as high as those on C1. In order to effectively improve the air quality of Taiyuan, we also should pay attention to the regional transport of pollutants on the basis of strengthening the local emission control.

Conclusion

In this study, the chemical composition, sources of $PM_{2.5}$, transport pathways, and potential source regions of air pollution were investigated before and during the COVID-19 outbreak in Taiyuan. The concentrations of $PM_{2.5}$ and its components decreased significantly during the epidemic outbreak due to the reduction of anthropogenic emission sources. However, two air pollution events still occurred during P2 when strict lockdown measures were implemented. The PMF model-resolved source analysis showed that VE, CC, SIA, DS, FB, and IP were the main sources of $PM_{2.5}$ in Taiyuan before and during the COVID-19 outbreak; except for fireworks burning, the air masses reaching Taiyuan from different potential geographical regions showed substantial reductions of the mass contributions from various sources. CWT results showed that the northwest of sampling sites, such as Shaanxi and Inner Mongolia, and the southwest of Shanxi Province were the main potential source regions. It is worth noting that the emission control of fireworks during the holidays should also be further controlled to prevent the occurrence of heavy pollution events. The emission reduction of vehicles has a significant impact on the improvement of air quality, and the development of clean energy should continue to be promoted. Due to the significant impact on the air quality of Taiyuan caused by regional transport, strict emission

Table 2 Average concentrations ($\mu g/m^3$) of six sources in cluster C1, C2, and C3 during P1 and P2

Cluster	Time	$PM_{2.5}$	VE	IP	DS	FB	SIA	CC
C1	P1	57.1	12.1	1.5	4.3	2.8	38.6	9.2
	P2	52.0	4.2	1.4	2.2	3.4	40.4	5.3
C2	P1	131.4	26.1	3.5	3.2	1.2	87.5	4.7
	P2	84.2	5.4	2.4	2.2	10.5	57.0	5.2
C3	P1	132.8	31.8	5.4	6.2	2.5	74.7	7.2
	P2	93.7	7.6	3.9	1.6	6.4	68.5	5.2

mitigation actions and joint measures to control air pollution should be enforced on the regional scale.

Data availability The datasets generated during and/or analyzed during the current study are available from the corresponding author on reasonable request.

Code availability Not applicable.

Declarations

Conflict of interest The authors declare no competing interests.

References

An J, Duan Q, Wang H, Miao Q, Shao P, Wang J, Zou J (2015). Fine particulate pollution in the Nanjing northern suburb during summer: composition and sources. Environ Monitor Assess 187 561. https://doi.org/10.1007/s10661-015-4765-2

Ashbaugh LL, Malm WC, Sadeh WZ (1985) A residence time probability analysis of sulfur concentrations at grand Canyon National Park. Atmos Environ 19:1263–1270. https://doi.org/10.1016/0004-6981(85)90256-2

Bond TC, Doherty SJ, Fahey DW, Forster PM, Berntsen T, DeAngelo BJ, Flanner MG, Ghan S, Kärcher B, Koch D, Kinne S, Kondo Y, Quinn PK, Sarofim MC, Schultz MG, Schulz M, Venkataraman C, Zhang H, Zhang S, Bellouin N, Guttikunda SK, Hopke PK, Jacobson MZ, Kaiser JW, Klimont Z, Lohmann U, Schwarz JP, Shindell D, Storelvmo T, Warren SG, Zender CS (2013) Bounding the role of black carbon in the climate system: a scientific assessment. J Geophys Res Atmos 118:5380–5552. https://doi.org/10.1002/jgrd.50171

Bressi M, Sciare J, Ghersi V, Mihalopoulos N, Petit JE, Nicolas JB, Moukhtar S, Rosso A, Féron A, Bonnaire N, Poulakis E, Theodosi C (2014) Sources and geographical origins of fine aerosols in Paris (France). Atmos Chem Physics 14:8813–8839. https://doi.org/10.5194/acp-14-8813-2014

Cao JJ, Lee SC, Chow JC, Watson JG, Ho KF, Zhang RJ, Jin ZD, Shen ZX, Chen GC, Kang YM, Zou SC, Zhang LZ, Qi SH, Dai MH, Cheng Y, Hu K (2007) Spatial and seasonal distributions of carbonaceous aerosols over China. J Geophys Res 112. https://doi.org/10.1029/2006jd008205

Cao JJ, Zhu CS, Tie XX, Geng FH, Xu HM, Ho SSH, Wang GH, Han YM, Ho KF (2013) Characteristics and sources of carbonaceous aerosols from Shanghai, China. Atmospheric Chemistry and Physics 13:803–817. https://doi.org/10.5194/acp-13-803-2013

Chu B, Zhang S, Liu J, Ma Q, He H (2021) Significant concurrent decrease in PM$_{2.5}$ and NO$_2$ concentrations in China during COVID-19 epidemic. J Environ Sci China 99:346–353. https://doi.org/10.1016/j.jes.2020.06.031

Cui Y, Ji D, Maenhaut W, Gao W, Zhang R, Wang Y (2020) Levels and sources of hourly PM$_{2.5}$-related elements during the control period of the COVID-19 pandemic at a rural site between Beijing and Tianjin. Sci Total Environ 744, 140840. https://doi.org/10.1016/j.scitotenv.2020.140840

Fan C, Li Y, Guang J, Li Z, Elnashar A, Allam M, de Leeuw G (2020) The impact of the control measures during the COVID-19 outbreak on air pollution in China. Remote Sens 12. https://doi.org/10.3390/rs12101613

Faridi S, Yousefian F, Niazi S, Ghalhari MR, Hassanvand MS, Naddafi K (2020) Impact of SARS-CoV-2 on ambient air particulate matter in Tehran. Aerosol Air Qual Res 20. https://doi.org/10.4209/aaqr.2020.05.0225

Huang RJ, Zhang Y, Bozzetti C, Ho KF, Cao JJ, Han Y, Daellenbach KR, Slowik JG, Platt SM, Canonaco F, Zotter P, Wolf R, Pieber SM, Bruns EA, Crippa M, Ciarelli G, Piazzalunga A, Schwikowski M, Abbaszade G, Schnelle-Kreis J, Zimmermann R, An Z, Szidat S, Baltensperger U, El Haddad I, Prevot AS (2014) High secondary aerosol contribution to particulate pollution during haze events in China. Nature 514:218–222. https://doi.org/10.1038/nature13774

Huang X, Liu Z, Liu J, Hu B, Wen T, Tang G, Zhang J, Wu F, Ji D, Wang L, Wang Y (2017) Chemical characterization and source identification of PM$_{2.5}$ at multiple sites in the Beijing–Tianjin–Hebei region China. Atmos Chem Physics 17:12941–12962. https://doi.org/10.5194/acp-17-12941-2017

Kim E, Larson TV, Hopke PK, Slaughter C, Sheppard LE, Claiborn C (2003) Source identification of PM$_{2.5}$ in an arid Northwest U.S. City by positive matrix factorization. Atmos Res 66:291–305. https://doi.org/10.1016/s0169-8095(03)00025-5

Kong SF, Li L, Li XX, Yin Y, Chen K, Liu DT, Yuan L, Zhang YJ, Shan YP, Ji YQ (2015) The impacts of firework burning at the Chinese Spring Festival on air quality: insights of tracers, source evolution and aging processes. Atmos Chem Phys 15:2167–2184. https://doi.org/10.5194/acp-15-2167-2015

Le T, Wang Y, Liu L, Yang J, Yung YL, Li G, Seinfeld JH (2020) Unexpected air pollution with marked emission reductions during the COVID-19 outbreak in China. Science 369. https://doi.org/10.1126/science.abb7431

Li H, Guo L, Cao R, Gao B, Yan Y, He Q (2016) A wintertime study of PM$_{2.5}$-bound polycyclic aromatic hydrocarbons in Taiyuan during 2009–2013: assessment of pollution control strategy in a typical basin region. Atmos Environ 140:404–414. https://doi.org/10.1016/j.atmosenv.2016.06.013

Li J, Li H, He Q, Guo L, Zhang H, Yang G, Wang Y, Chai F (2020a) Characteristics, sources and regional inter-transport of ambient volatile organic compounds in a city located downwind of several large coke production bases in China. Atmospheric Environment 233. https://doi.org/10.1016/j.atmosenv.2020.117573

Li P, Yan R, Yu S, Wang S, Liu W, Bao H (2015). Reinstate regional transport of PM$_{2.5}$ as a major cause of severe haze in Beijing. Proc Nat Acad Sci 112. https://doi.org/10.1073/pnas.1502596112

Li R, Zhao Y, Fu H (2020b). substantial changes of gaseous pollutants and chemical composition in fine particles in North China. Atmos Chem Phys. 10.5194/acp-2020-1199

Liu K, Wang S, Wu Q, Wang L, Ma Q, Zhang L, Li G, Tian H, Duan L, Hao J (2018) A Highly Resolved Mercury Emission Inventory of Chinese Coal-Fired Power Plants. Environ Sci Technol 52:2400–2408. https://doi.org/10.1021/acs.est.7b06209

Liu Y, Zheng M, Yu M, Cai X, Du H, Li J, Zhou T, Yan C, Wang X, Shi Z, Harrison RM, Zhang Q, He K (2019) High-time-resolution source apportionment of PM$_{2.5}$ in Beijing with multiple models. Atmos Chemis Phys 19:6595–6609. https://doi.org/10.5194/acp-19-6595-2019

Lyu X, Chen N, Guo H, Zeng L, Zhang W, Shen F, Quan J, Wang N (2016) Chemical characteristics and causes of airborne particulate pollution in warm seasons in Wuhan, central China. Atmos Chem Phys 16:10671–10687. https://doi.org/10.5194/acp-16-10671-2016

Na Z, Gang W, Guohao L, Jianlei L, Hanyu Z (2020) Air pollution episodes during the COVID-19 outbreak in the Beijing–Tianjin–Hebei region of China: an insight into the transport pathways and source distribution. Environ Pollut 267. https://doi.org/10.1016/j.envpol.2020.115617

Navinya C, Patidar G, Phuleria HC (2020) Examining effects of the COVID-19 national lockdown on ambient air quality across urban India. Aerosol Qual Res 20. https://doi.org/10.4209/aaqr.2020.05.0256

Qi Y, Bing Q, Deyun H, Junjiao W, Jian Z, Huanqiang Y, Shanshan Z, Lei L, Liang X, Weijun L (2021) Spatiotemporal variations and reduction of air pollutants during the COVID-19 pandemic in a megacity of Yangtze River Delta in China. Sci Total Environ 751. https://doi.org/10.1016/j.scitotenv.2020.141820

Rai P, Furger M, Slowik JG, Canonaco F, Fröhlich R, Hüglin C, Minguillón MC, Petterson K, Baltensperger U, Prévôt ASH (2020) Source apportionment of highly time-resolved elements during a firework episode from a rural freeway site in Switzerland. Atmos Chem Phys 20:1657–1674. https://doi.org/10.5194/acp-20-1657-2020

Reff A, Eberly SI, Bhave PV (2007) Receptor modeling of ambient particulate matter data using positive matrix factorization: review of existing methods. J Air Waste Manag Assoc 57. https://doi.org/10.1080/10473289.2007.10465319

RoigRodelas R, Perdrix E, Herbin B, Riffault V (2019) Characterization and variability of inorganic aerosols and their gaseous precursors at a suburban site in northern France over one year (2015–2016). Atmos Environ 200:142–157. https://doi.org/10.1016/j.atmosenv.2018.11.041

Schauer JJ, Kleeman MJRCG (2002) Measurement of emissions from air pollution sources. 5. C1-C32 Organic Compounds from Gasoline-Powered Motor Vehicles. Environ Sci Technol 1169-1180. https://doi.org/10.1021/es0108077

Su C-P, Peng X, Huang X-F, Zeng L-W, Cao L-M, Tang M-X, Chen Y, Zhu B, Wang Y, He L-Y (2020) Development and application of a mass closure PM$_{2.5}$ composition online monitoring system. Atmos Meas Tech 13:5407–5422. https://doi.org/10.5194/amt-13-5407-2020

Sun Y, Guo S, Tang A, Wang Y, An Z (2006) Chemical characteristics of PM$_{2.5}$ and PM$_{10}$ in haze-fog episodes in Beijing. Environ Sci Technol 3148–3155. https://doi.org/10.1021/es051533g

Taiwo AM, Harrison RM, Shi Z (2014) A review of receptor modelling of industrially emitted particulate matter. Atmos Environ 97:109–120. https://doi.org/10.1016/j.atmosenv.2014.07.051

Tian HZ, Zhu CY, Gao JJ, Cheng K, Hao JM, Wang K, Hua SB, Wang Y, Zhou JR (2015) Quantitative assessment of atmospheric emissions of toxic heavy metals from anthropogenic sources in China: historical trend, spatial distribution, uncertainties, and control policies. Atmos Chem Phys 15:10127–10147. https://doi.org/10.5194/acp-15-10127-2015

Turpin BJ, Lim H-J (2001) Species contributions to PM2.5 mass concentrations: revisiting common assumptions for estimating organic mass aerosol. Sci Technol 35:602–610. https://doi.org/10.1080/02786820119445

Wang P, Chen K, Zhu S, Wang P, Zhang H (2020) Severe air pollution events not avoided by reduced anthropogenic activities during COVID-19 outbreak. Res Conserv Recycling 158, 104814. https://doi.org/10.1016/j.resconrec.2020.104814

Wang S, Zhang Y, Ma J, Zhu S, Shen J, Wang P, Zhang H (2021). Responses of decline in air pollution and recovery associated with COVID-19 lockdown in the Pearl River Delta. Sci Total Environ 756 143868. https://doi.org/10.1016/j.scitotenv.2020.143868

Wang YQ, Zhang XY, Draxler RR (2009) TrajStat: GIS-based software that uses various trajectory statistical analysis methods to identify potential sources from long-term air pollution measurement data. Environ Model Softw 24:938–939. https://doi.org/10.1016/j.envsoft.2009.01.004

Wu Z, Hu M, Shao K, Slanina J (2009) Acidic gases, NH$_3$ and secondary inorganic ions in PM$_{10}$ during summertime in Beijing, China and their relation to air mass history. Chemosphere 76:1028–1035. https://doi.org/10.1016/j.chemosphere.2009.04.066

Xia L, Gao Y (2011) Characterization of trace elements in PM2.5 aerosols in the vicinity of highways in northeast New Jersey in the U.S. east coast. Atmos Pollut Res 2:34–44. https://doi.org/10.5094/apr.2011.005

Yao L, Yang L, Yuan Q, Yan C, Dong C, Meng C, Sui X, Yang F, Lu Y, Wang W (2016) Sources apportionment of PM$_{2.5}$ in a background site in the North China Plain. Sci Total Environ 541:590–598. https://doi.org/10.1016/j.scitotenv.2015.09.123

Zhang J, Cui K, Wang Y-F, Wu J-L, Huang W-S, Wan S, Xu K (2020a) Temporal variations in the air quality index and the impact of the COVID-19 event on air quality in western China aerosol and air quality research 20. https://doi.org/10.4209/aaqr.2020.06.0297

Zhang R, Zhang Y, Lin H, Feng X, Fu T-M, Wang Y (2020b) NOx emission reduction and recovery during COVID-19 in East China. Atmosphere 11. https://doi.org/10.3390/atmos11040433

Zhang Z, Cui Y, He Q, Guo L, Tian X, Zhang K, Wang X (2020) Predominant effects of emission reduction by recording 8-year water-soluble ions in precipitation in Taiyuan, North China. Atmos Pollut Res 11:1922–1932. https://doi.org/10.1016/j.apr.2020.08.004

Zheng GJ, Duan FK, Su H, Ma YL, Cheng Y, Zheng B, Zhang Q, Huang T, Kimoto T, Chang D, Pöschl U, Cheng YF, He KB (2015) Exploring the severe winter haze in Beijing: the impact of synoptic weather, regional transport and heterogeneous reactions. Atmos Chem Phys 15:2969–2983. https://doi.org/10.5194/acp-15-2969-2015

Zheng H, Kong S, Chen N, Yan Y, Liu D, Zhu B, Xu K, Cao W, Ding Q, Lan B, Zhang Z, Zheng M, Fan Z, Cheng Y, Zheng S, Yao L, Bai Y, Zhao T, Qi S (2020) Significant changes in the chemical compositions and sources of PM$_{2.5}$ in Wuhan since the city lockdown as COVID-19. Sci Total Environ 739 140000. https://doi.org/10.1016/j.scitotenv.2020.140000

Zheng H, Kong S, Yan Q, Wu F, Cheng Y, Zheng S, Wu J, Yang G, Zheng M, Tang L, Yin Y, Chen K, Zhao T, Liu D, Li S, Qi S, Zhao D, Zhang T, Ruan J, Huang M (2019) The impacts of pollution control measures on PM$_{2.5}$ reduction: insights of chemical composition, source variation and health risk. Atmos Environ 197:103–117. https://doi.org/10.1016/j.atmosenv.2018.10.023

Publisher's Note Springer Nature remains neutral with regard to jurisdictional claims in published maps and institutional affiliations.